



Elasto-Plastic Stress States and Reduced Flexural Stiffness of Steel Beam-Columns

Barry T. Rosson¹

Abstract

The stiffness reduction that results from yielding of the cross-section due to minor axis bending and axial compression is studied in detail for compact W-Shapes with a European Convention for Constructional Steelwork (ECCS) residual stress distribution pattern. For a given minor axis moment m (M/M_p), compressive load p (P/P_y), and residual stress ratio c_r (σ_r/σ_y), the distribution of stresses throughout the cross-section and associated reduced stiffness τ (EI_{ep}/EI) are evaluated using a fiber element model with 2,046 elements. A three-dimensional m - p - τ surface plot of a W8x31 with $c_r = 0.3$ is used to discuss the stress states and reduced stiffness for the m and p conditions around the perimeter of the surface. For these conditions, equations that predict the extent of yielding and the distribution of stresses in the flanges and web are provided for any given W-Shape and c_r condition. The ability to determine the stresses with analytical expressions leads to reduced stiffness equations that are no longer dependent upon empirical relationships. Seven elasto-plastic stress states have been identified for the m and p conditions on the interior of the surface. Discussion is provided on the development of similar analytical expressions for these conditions. Numerous figures are provided on the progression through the various stress states as m is increased from the initial yield condition up to the fully plastic state for $p = 0.2, 0.5$ and 0.75 . The data from the m - p - τ surface plot for the W8x31 with minor axis bending are used to develop two nonlinear regression equations for use as tangent modulus expressions in *MASTAN2*. The El-Zanaty portal frame is modeled with $p = 0.4$ and 0.6 . The maximum lateral load and deflection values compared very closely with published results of the same frame under similar conditions.

1. Introduction

The in-plane behavior of steel frames with compact doubly-symmetric members that are subjected to minor axis bending have been shown to exhibit significant differences in their response based on plastic hinge and plastic zone analyses (Ziemian et al. 2002). Frames of this type with little to no redundancy can be very sensitive to the refinement of the inelastic analysis procedure employed (El-Zanaty et al. 1980; White et al. 1991; Ziemian et al. 1997). Recent research has focused on developing improved empirical relationships to account for the reduction in stiffness that occurs due to yielding of the cross-section from minor axis axial bending and axial compression (Zubydan 2011; Kucukler et al. 2014). The objective of this paper is to present the findings from a detailed

¹ Professor, Florida Atlantic University, <rosson@fau.edu>

fiber element model investigation of the stresses and stiffness reduction that develop as a result of yielding in the flanges and web over the full range of moment and axial load combinations from initial yield to the fully plastic condition. Analytical expressions are presented to determine the extent of yielding and stiffness reduction for key stress state conditions, and discussion is provided on how the methodology can be used to consider the seven elasto-plastic stress states identified in the study. Finally, the paper presents an approximation of the stiffness reduction using two nonlinear regression equations, and discusses how it can be used effectively in a nonlinear analysis program such as *MASTAN2* to obtain results that are comparable with those from a more detailed distributed plasticity approach.

2. Fiber Element Model

The stiffness reduction that results from yielding of the cross-section due to minor axis bending up to the plastic moment M_p and axial compression up to the yield load P_y is studied in detail for W-Shapes with an ECCS residual stress pattern (1984) as depicted in Fig. 1. For a given normalized minor axis moment m (M/M_p), compressive load p (P/P_y), and residual stress ratio c_r (σ_r/σ_y), the stiffness reduction and distribution of normal stress throughout the cross-section were carefully assessed using a detailed fiber element model of a W8x31 with $c_r = 0.3$.

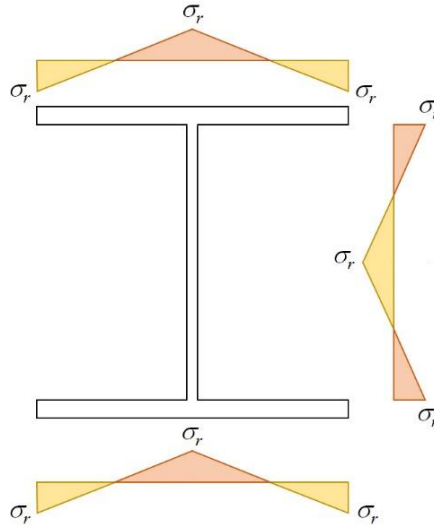


Figure 1: Residual stress pattern used in the study

A computer program was developed to accommodate a specified number of rows and columns of fiber elements in each flange and the web. The angle and location of linear strain distribution were varied in specified increments from zero to specified maximums in order to capture the m and p conditions at 0.01 increments to at least three significant digits of accuracy. The final model used 2,046 fiber elements over the cross-section (400 fiber elements in each flange and 1,246 fiber elements in the web). This level of discretization was found to be necessary to develop the smooth m - p - τ surface plot in Fig. 2. Using the m and p results with increments of 0.01, a total of 7,590 data points were used to produce the 3D surface plot (m and p combinations of $\tau = 0$ outside the boundary were excluded). A triangular shaped plateau of $\tau = 1$ is observed, and the loss of stiffness to $\tau = 0$ varies dramatically depending upon the magnitudes of both m and p . For the lower values of p between 0 and approximately 0.2, the loss of stiffness is more gradual for a given increment of m beyond the edge of the plateau. With the same increment of m for p between 0.2 and 0.7, the

loss of stiffness is more rapid immediately adjacent the ridge of the plateau. For the higher values of p between 0.7 and 1, the surface plot takes on a very different shape with a smooth, distinct fold at values of m between 0 and approximately 0.1. For $m = 0$ and $p > 0.7$ the shape of the curve is convex, and for a given increment of p there is a rapid decrease in stiffness to $\tau = 0$.

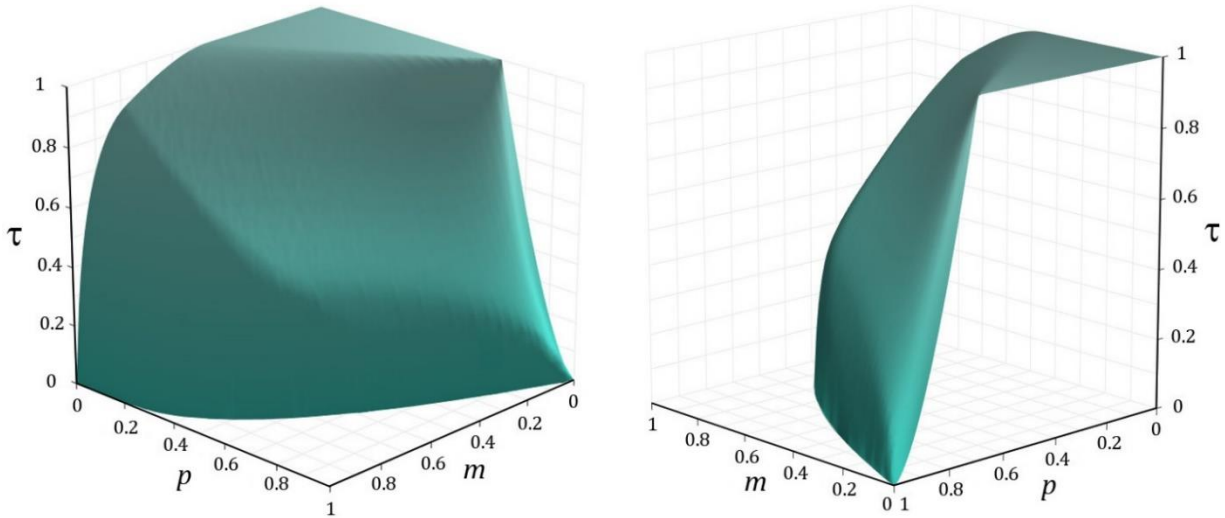


Figure 2: m - p - τ surface plot for minor axis bending of a W8x31 with $c_r = 0.3$

3. Stress State Conditions Around the Perimeter of the Surface Plot

As depicted in Fig. 3, there are four unique conditions around the perimeter of the surface plot. The next section will discuss the stress states for each of the four conditions, and equations will be given to determine the extent of yielding of the cross-section and the corresponding stiffness reduction.

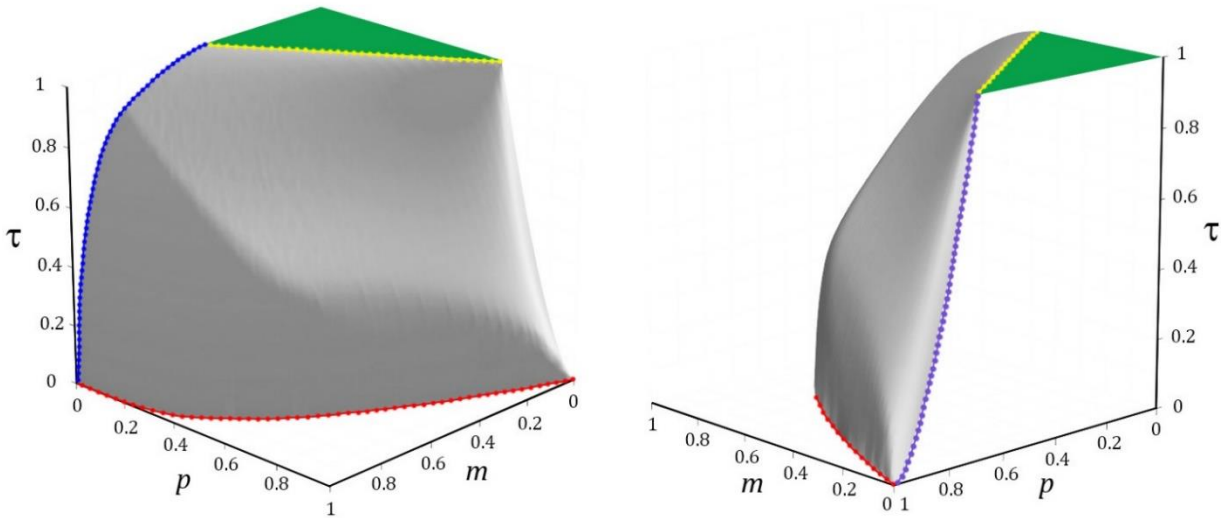


Figure 3: Four unique conditions around the perimeter of the m - p - τ surface plot

3.1 Yellow line in Fig. 3 (m and p conditions at the limit of $\tau = 1$)

The equation to determine the extent of $\tau = 1$ is found in the literature (Zubydan 2011) and is straight-forward to visualize as depicted in Fig. 4. The dashed blue lines represent the residual

stress distribution, and the shaded regions represent the compressive stresses (left) and tensile stresses (right) due to the minor axis bending moment and axial compression load. The left side of the diagram depicts the accumulation of three stresses: the bending moment compressive stress σ_m , the axial compressive stress σ_p , and the residual compressive stress σ_r . The extent of $\tau = 1$ is determined when the conditions of m and p cause all three compressive stresses to sum to σ_y . Z_y is the minor axis plastic section modulus and S_y is the minor axis elastic section modulus.

$$\frac{Z_y}{S_y}m + p + c_r = 1 \quad (1)$$

Fig. 4 provides the stress states for two axial loads at which the extent of $\tau = 1$ is reached. For the conditions of $p = 0.2$ and 0.5 , the compression yield is reached on the left side when $m = 0.329$ and 0.132 , respectively. For $p = 0.5$, compressive stresses occur over the full flange width b_f .

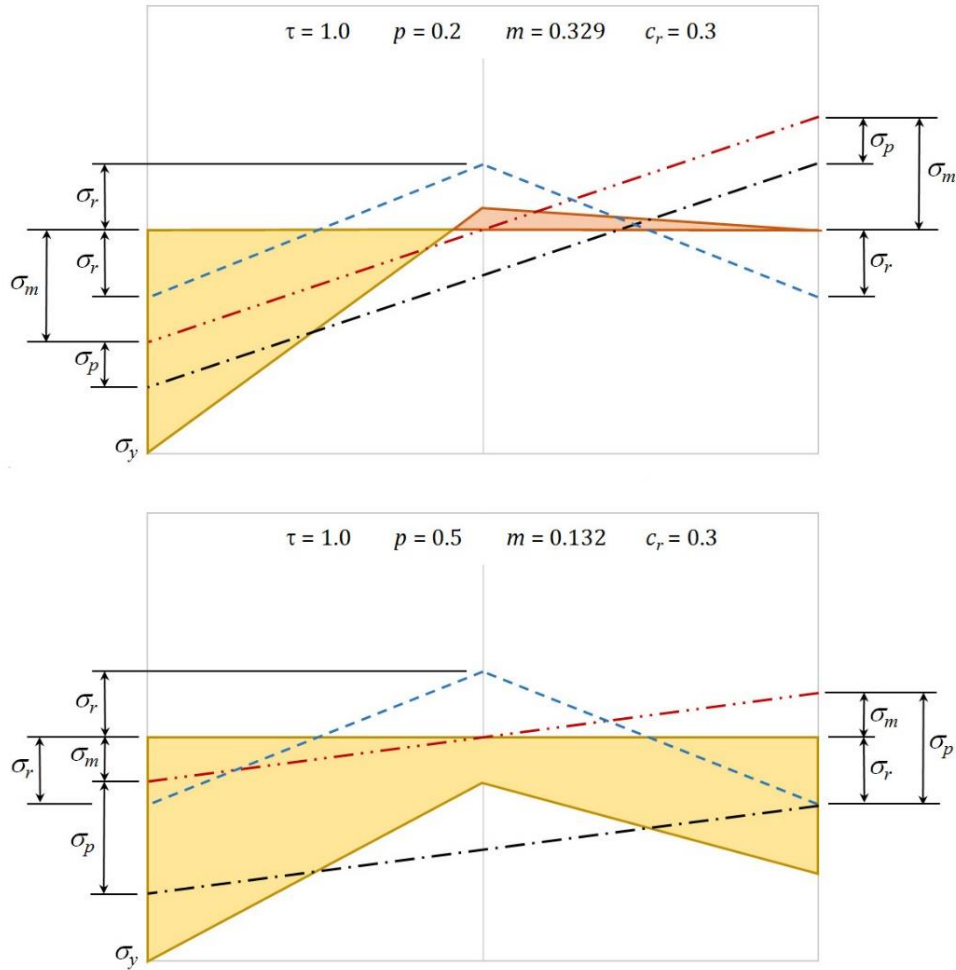


Figure 4: Stress states in the flanges at the extent of $\tau = 1$ for $p = 0.2$ and 0.5

3.2 Blue line in Fig. 3 ($p = 0$ and m conditions for $0 < \tau < 1$)

For a given of elasto-plastic moment M_{ep} , the cross-section has a specific value of reduced flexural stiffness EI_{ep} . Recognizing that plane sections remain plane after bending, even after a portion of the cross-section has yielded, the curvature equation is given as

$$\phi = \frac{M_{ep}}{EI_{ep}} = \frac{M_{ep}}{\tau EI_y} \quad (2)$$

The bending moment M_1 is defined to be the moment that would exist if the section had not yielded and maintained its full stiffness EI_y . With this condition of moment, the curvature is defined to be the same as the actual condition of moment M_{ep} with reduced stiffness EI_{ep} .

$$\phi = \frac{M_1}{EI_y} = \frac{M_{ep}}{EI_{ep}} \quad (3)$$

From Eqs. 2 and 3, the relationship for τ in terms of the moments M_{ep} and M_1 is given as

$$\tau = \frac{M_{ep}}{M_1} \quad (4)$$

In Fig. 5, the dashed red line represents the stress distribution due to the moment M_1 , and its slope is given as

$$s_1 = \frac{\sigma_o}{h_o} = \frac{M_1}{I_y} \quad (5)$$

The moment M_1 is evaluated using the stresses σ_{le} and σ_{re} in Fig. 5. The slopes of the two lines of the shaded regions are related to s_1 by the residual stresses on the left and right sides of the centerline, and are given as

$$s_L = \frac{\sigma_o}{h_o} + \frac{4\sigma_r}{b_f} \quad (6)$$

$$s_R = \frac{\sigma_o}{h_o} - \frac{4\sigma_r}{b_f} \quad (7)$$

Ignoring for the moment the effect of the web, the condition of pure bending ($p = 0$) is achieved when the areas of the two shaded regions are equal. The resulting bending moment is determined by considering both flanges and summing the moments of the two shaded regions acting over the flange thickness t_f . When this calculated moment is equal to the actual M_{ep} moment, the correct stress state has been determined and the stiffness reduction τ can be evaluated.

One would normally need to use an iterative procedure with σ_o and h_o to find the correct shaded areas that satisfy the conditions above; however, when excluding the effect of the web, the stiffness reduction can be determined directly using Eq. 8 for a given m and c_r condition.

$$\tau = \frac{m}{\frac{4}{3} \left[\frac{8(1+c_r)^3}{(6+2c_r-3m)^2} - c_r \right]} \quad (8)$$

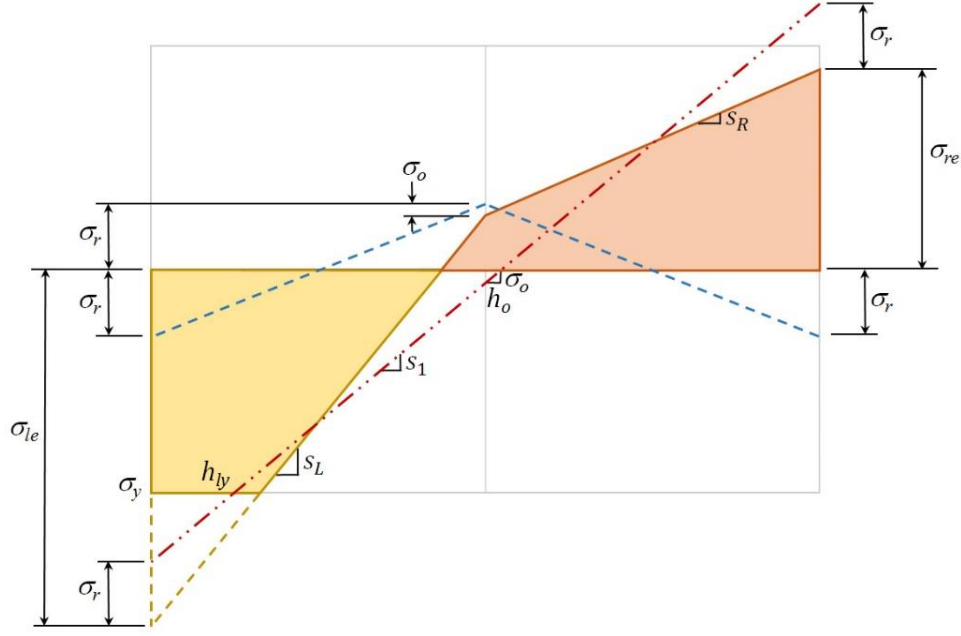


Figure 5: Stresses in the flanges for $p = 0$ and m producing only compression yield

The extent of yielding along the width of each flange h_{ly} can also be evaluated directly using

$$h_{ly} = b_f \left[\frac{3m + 2c_r - 2}{4(1 + c_r)} \right] \quad (9)$$

The expression for τ can be determined for the condition in which the web effect is included; however, it is no longer in closed form as in Eq. 8. An iterative approach is first needed to determine the value of σ_o such that the M_{ep} calculated in Eq. 10 is equal to the actual elasto-plastic moment to within a given tolerance.

$$M_{ep} = \frac{M_y}{B_0} \left[2 + B_0 + c_r(2 - B_0) + \frac{\sigma_o}{\sigma_y} (2B_1 - B_0B_2) \right] \quad (10)$$

Using the ratios $\lambda = A_w/A_f$ and $\lambda_o = t_w/b_f$

$$B_0 = 1 + \sqrt{\frac{\lambda + 2\sigma_y \left(\frac{1 + c_r}{\sigma_o} \right)}{\lambda + 2}} \quad (11)$$

$$B_1 = \frac{\lambda(1 - \lambda_o^2)}{2 + \lambda\lambda_o^2} \quad (12)$$

$$B_2 = \frac{-\lambda(1 + 2\lambda\lambda_o^2 + 3\lambda_o^2)}{2 + \lambda\lambda_o^2} \quad (13)$$

The stiffness reduction is determined using the final value of σ_o from the iterative procedure described above.

$$\tau = \frac{m}{\frac{S_y}{Z_y} \left[\frac{B_0^2 \sigma_o}{2\sigma_y} (\lambda + 2) - 2c_r \right]} \quad (14)$$

The extent of yielding along the width of each flange h_{ly} is evaluated using

$$h_{ly} = \frac{b_f}{B_0} \quad (15)$$

As the bending moment increases, the tensile stresses on the right side exceed the yield stress as illustrated in Fig. 6. Additional equations are needed to determine the stiffness reduction and the widths over which yielding occurs on the left and right sides of each flange (h_{ly} and h_{ry}). As before, the solution is first considered excluding the effect of the web. For this particular condition, the stiffness reduction can be determined directly using

$$\tau = \frac{m}{\frac{2}{3} \sqrt{\frac{1}{3(1-m) + 9c_r^2(1-m)^2 + 4c_r^2}}} \quad (16)$$

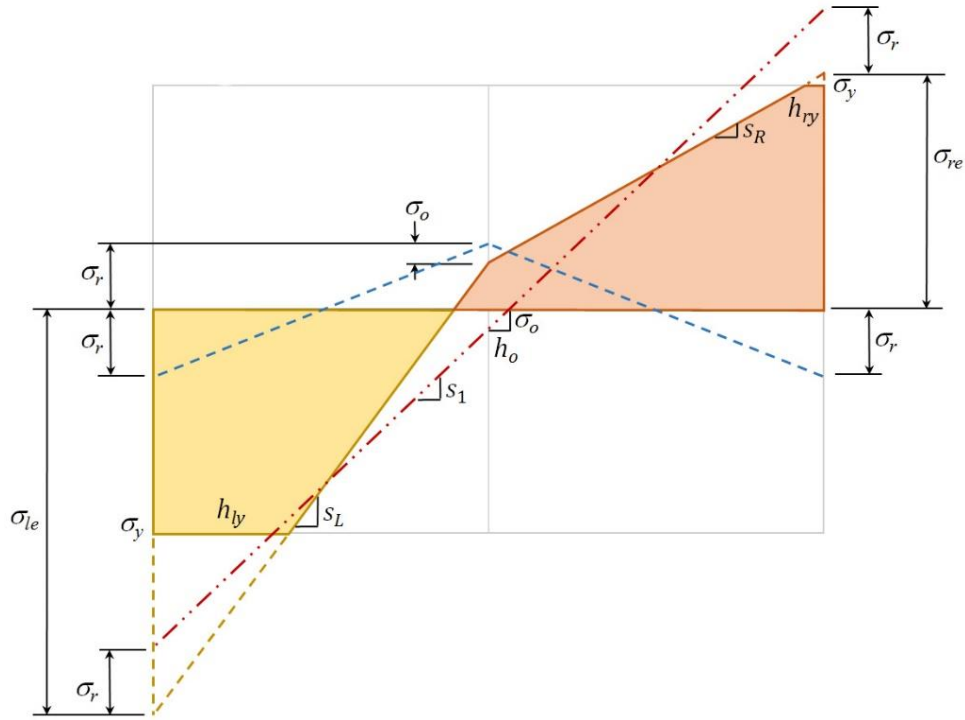


Figure 6: Stresses in the flanges for $p = 0$ and m producing compression and tension yield

The extent of yielding along the width of each flange h_{ly} and h_{ry} can be evaluated directly using

$$h_{ly} = \frac{b_f}{2} \left[1 - \frac{1 + \frac{1}{\sqrt{3c_r^2(1-m)} + 1}}{\frac{1.5m}{\tau} + 2c_r} \right] \quad (17)$$

$$h_{ry} = \frac{b_f}{2} \left[1 - \frac{1 - \frac{1}{\sqrt{3c_r^2(1-m)} + 1}}{\frac{1.5m}{\tau} - 2c_r} \right] \quad (18)$$

The stiffness reduction can be evaluated for the condition in which the web effect is included; however, as before it is no longer in closed form and an iterative approach is needed to determine the correct σ_o value for a given M_{ep} condition.

$$M_{ep} = [s_1 B_3 + B_4(1.5\sigma_y - B_5 - B_6)] I_y \quad (19)$$

$$B_3 = \frac{\lambda \lambda_o^2}{2 + \lambda \lambda_o^2} \quad (20)$$

$$B_4 = \frac{4}{b_f(2 + \lambda \lambda_o^2)} \quad (21)$$

$$B_5 = \frac{\sigma_y \left(1 - c_r + \frac{\sigma_o}{\sigma_y}\right)^3}{\left(\frac{s_1 b_f}{\sigma_y} - 4c_r\right)^2} \quad (22)$$

$$B_6 = \frac{\sigma_y \left(1 + c_r - \frac{\sigma_o}{\sigma_y}\right)^3}{\left(\frac{s_1 b_f}{\sigma_y} + 4c_r\right)^2} \quad (23)$$

$$s_1 = \frac{2\sigma_y^2 \left(c_r - \frac{\sigma_o}{\sigma_y}\right)}{\sigma_o b_f \lambda} \pm \sqrt{4 \left[\frac{\sigma_y^2 \left(c_r - \frac{\sigma_o}{\sigma_y}\right)}{\sigma_o b_f \lambda} \right]^2 - B_7} \quad (24)$$

$$B_7 = \frac{8\sigma_y c_r}{\sigma_o b_f^2 \lambda} \left[\sigma_y^2 \left(1 + c_r^2 + \frac{\sigma_o^2}{\sigma_y^2} \right) - 2\sigma_o \sigma_y c_r (1 + \lambda) \right] \quad (25)$$

Once σ_o is determined to within a given tolerance, the s_1 value from Eq. 24 is used to determine τ in the following equation.

$$\tau = \frac{M_{ep}}{s_1 I_y} \quad (26)$$

The yield widths in each flange h_{ly} and h_{ry} are determined using the following relationships.

$$h_{ly} = \frac{b_f}{2} - \frac{1 + c_r - \frac{\sigma_o}{\sigma_y}}{\frac{s_1}{\sigma_y} + \frac{4c_r}{b_f}} \quad (27)$$

$$h_{ry} = \frac{b_f}{2} - \frac{1 - c_r + \frac{\sigma_o}{\sigma_y}}{\frac{s_1}{\sigma_y} - \frac{4c_r}{b_f}} \quad (28)$$

Considering a W8x31 with $c_r = 0.3$, the τ results obtained from Eqns. 8 and 16 (web excluded) are compared with those from Eqns. 14 and 26 (web included). As indicated in Fig. 7, the τ results are very similar across the full range of minor axis bending moments from the initial yield condition up to the plastic moment condition.

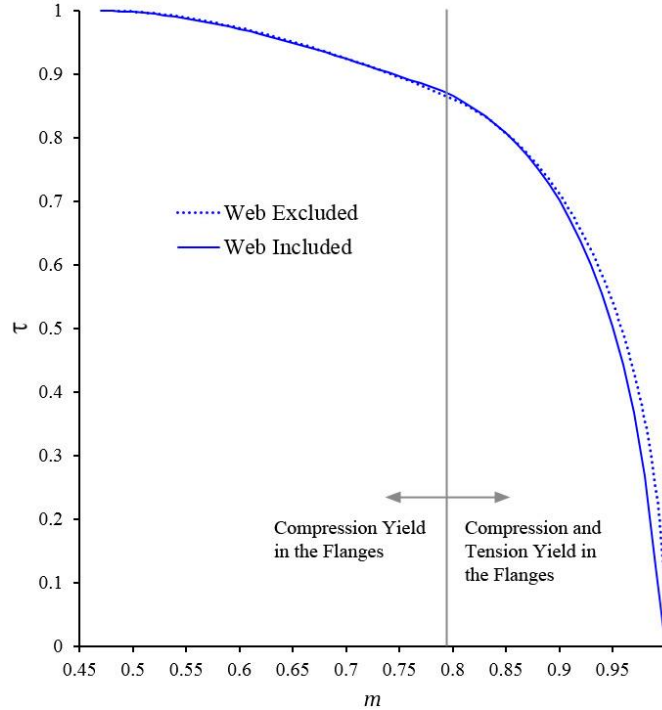


Figure 7: Comparison of m - τ results for Eqns. 8 & 16 (web excluded) and Eqns. 14 & 26 (web included) for $p = 0$

The results obtained from Eqns. 14 and 26 match the fiber element model results to at least three significant digits of accuracy; thus the blue line in Fig. 3 is essentially the same curve as the solid blue line in Fig. 7.

3.3 Purple line in Fig. 3 ($m = 0$ and p conditions for $0 < \tau < 1$)

The equation to determine the stiffness reduction when $m = 0$ is found by considering the stress state depicted in Fig. 8. The compressive stress σ_p' that satisfies the equilibrium condition for a given p and c_r condition provides the necessary information to determine the extent of yielding over the length h_y at the ends of the flanges and over the length $2h_y$ at the center of the web. The length h_y is determined using Eq. 29 where $d = b_f$ for yielding in the flanges and $d = d_w$ for yielding in the web.

$$h_y = \frac{d}{2} \left(1 - \sqrt{\frac{1-p}{c_r}} \right) \quad (29)$$

To determine the stiffness reduction τ for a given p and c_r condition, the minor axis moment of inertia of the remaining cross-section that has not yielded is divided by the original minor axis moment of inertia I_y .

$$\tau = \frac{2 \left(\frac{1-p}{c_r} \right)^{3/2} + \lambda \lambda_o^2 \left(\frac{1-p}{c_r} \right)^{1/2}}{2 + \lambda \lambda_o^2} \quad (30)$$

For W-Shapes in which $\lambda \lambda_o^2$ is very small compared to 2, excluding the effect of the web provides a very close approximation (e.g, W8x31 $\lambda \lambda_o^2 = 7.4 \times 10^{-4}$).

$$\tau = \left(\frac{1-p}{c_r} \right)^{3/2} \quad (31)$$

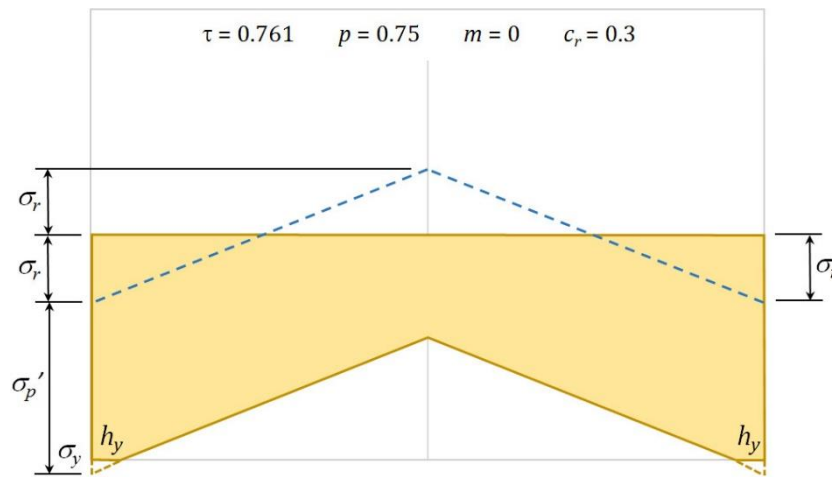


Figure 8: Stress state in the flanges for $p = 0.75$ and $m = 0$

Zubydan (2011) provides an empirical relationship of $4.88p^2 - 11.84p + 6.9$ that is within a 3% relative error of Eq. 30 for $0.7 < p < 0.93$ and $c_r = 0.3$.

3.4 Red line in Fig. 3 (m and p conditions for $\tau = 0$)

Two equations are needed to determine the m and p conditions when $\tau = 0$. One equation is needed when the plastic neutral axis is inside the web thickness, and the other is needed when it is outside the web thickness. The two closed-form equations are given in the book by Chen and Sohal (1995). When using the ratios $\lambda = A_w/A_f$, $\lambda_o = t_w/b_f$ and $\lambda_1 = d_w/t_f$, the same results are obtained with slightly fewer computations.

$$\frac{p^2(2 + \lambda)^2}{(2 + \lambda\lambda_o)(2 + \lambda_1)} + m = 1 \quad (32)$$

$$\text{when } p \geq \frac{2\lambda_o + \lambda}{2 + \lambda} \quad \frac{[p(2 + \lambda) - \lambda]^2}{4} + \frac{(2 + \lambda\lambda_o)m}{2} = 1 \quad (33)$$

4. Elasto-Plastic Stress State Conditions

As indicated in Table 1, there are seven elasto-plastic stress states between the initial yield condition and the fully plastic condition. The discussion of Figs. 5 and 6 explored stress states 1 and 2 for the special case of $p = 0$. As the axial compression load is increased from zero, stress states 1 and 2 continue to exist until yielding occurs at the center of the web to produce stress states 3 and 4. When the axial compression load is increased even further, the entire web yields in compression to produce stress states 5 and 6. The discussion of Fig. 8 explored stress state 7 for the special case of $m = 0$. For a range of small moments, stress state 7 remains in effect and is observed to occur in the folded region of the surface plot adjacent to the purple line in Fig. 3.

Table 1: Stress states with corresponding yield conditions in the flanges and web

Stress State ¹	Flanges		Web		
	Left	Right	Top	Middle	Bottom
SS 0	Elastic		Elastic		
SS 1	C				
SS 2	C	T			
SS 3	C			C	
SS 4	C	T		C	
SS 5	C		C	C	C
SS 6	C	T	C	C	C
SS 7	C	C		C	
SS 8	Plastic		Plastic		

1. C = Compression yield T = Tension yield

For axial load conditions of $p = 0.2, 0.5$ and 0.75 , Fig. 9 illustrates the progression through the various stress states as m is increased from the initial yield condition up to the fully plastic condition. There is a particular order of progression through the stress states for each axial load condition, and whereas the progressions for $p = 0.2$ and 0.5 are similar, the stress state progressions for $p = 0.75$ are quite different.

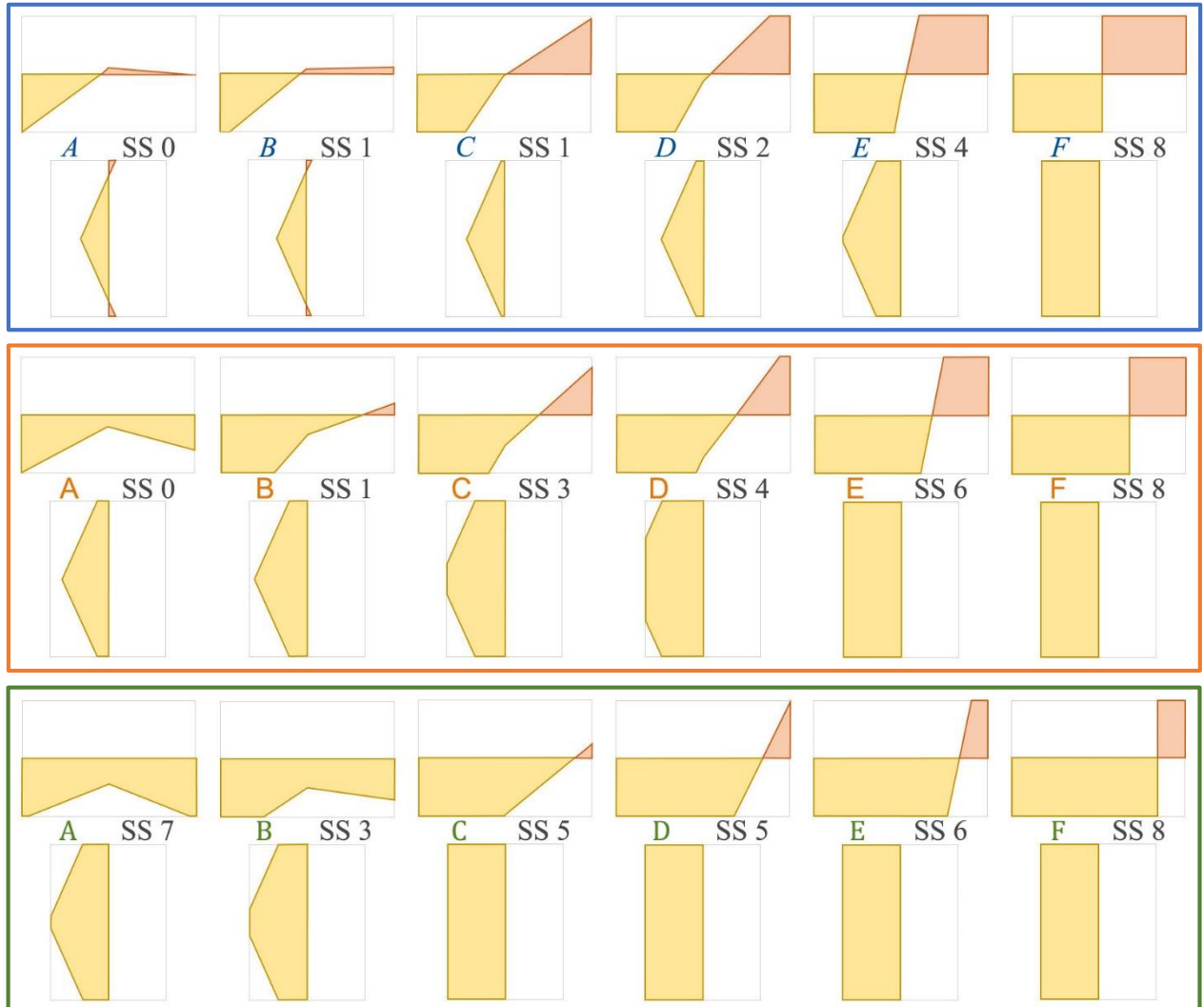
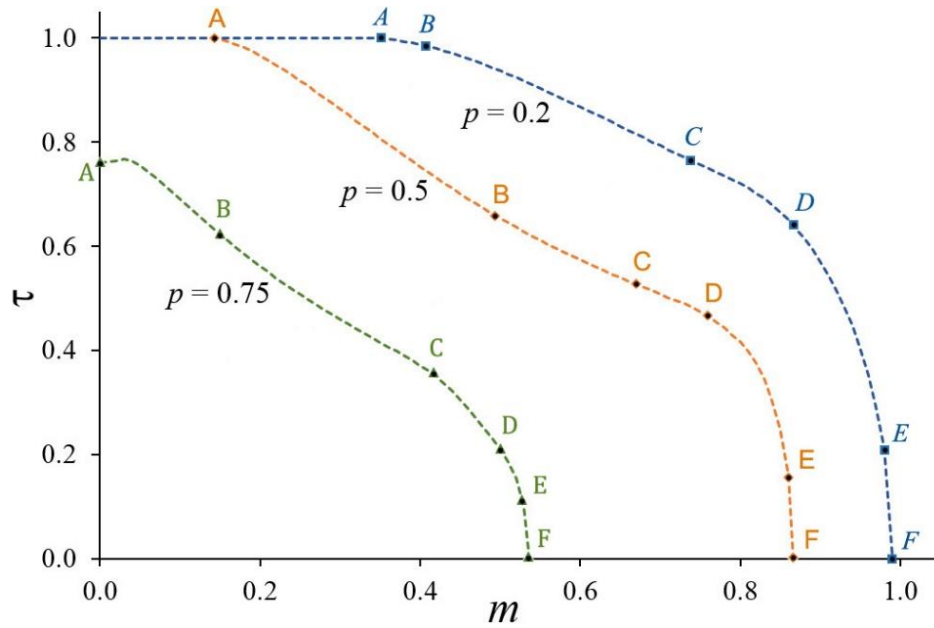


Figure 9: m - τ curves and stress state illustrations at points A through F for $p = 0.2, 0.5$ and 0.75

Fig. 9 is helpful with understanding how the stiffness reduction occurs as the minor axis moments are increased for a given axial load condition. For a given increment of m from the initial yield condition, the loss of stiffness occurs more rapidly as p is increased (points A through D). The loss of stiffness occurs most rapidly for all conditions of p when the flanges yield in both compression and tension (points D through F).

In order to develop the analytical expressions for stress states 1 through 7, σ_p' is introduced to account for the axial compression load. Fig. 10 illustrates the stresses in the flanges for the general stress state 2 condition when $p > 0$. Comparing the stresses in the flanges in Fig. 5 (with $p = 0$) with those in Fig. 10 for the same slope condition s_1 , it is noticed that additional compression yield occurs on the left side and the tension stresses are reduced on the right side. For a given moment and axial load that produces a particular stress state 2 condition, all the variables in Fig. 10 can be evaluated using the appropriate equations of equilibrium.

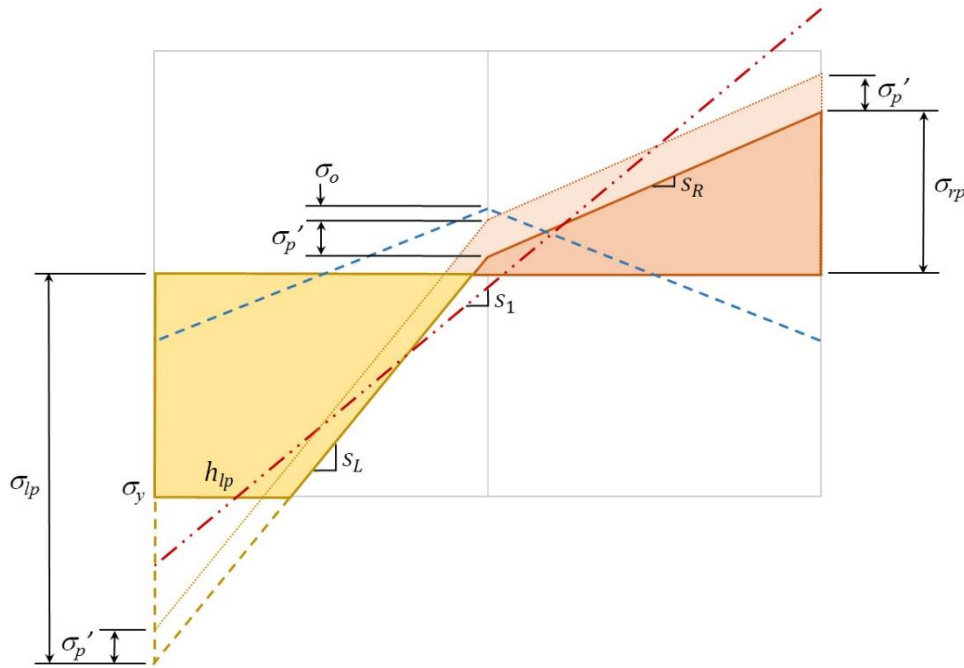


Figure 10: Stresses in the flanges for $p > 0$ and m producing compression yield

For stress states 3 and 4, compression yield occurs in the middle of the web as illustrated in Fig. 11. The extent of yielding l_{yw} can be determined for these two stress states using

$$l_{yw} = \frac{d_w}{2} \left[1 + \frac{\sigma_p' + \sigma_o}{c_r \sigma_y} - \frac{1}{c_r} \right] \quad (34)$$

Unfortunately due to space limitations, the general analytical equations for stress states 1 through 7 cannot be provided here because they are of length and form similar to Eqs. 10 through 15 and Eqs. 19 through 28. A full-length journal paper containing all the analytical equations is currently being finalized. The equations to determine the extent of yielding, and the distribution of stresses in the flanges and web, were found to be accurate to at least three significant digits of accuracy

when compared with the detailed fiber element model results over the full range of m - p - τ conditions in Fig. 3. The ability to determine these stresses over the cross-section of a W-Shape at any given m , p and c_r condition leads to reduced stiffness equations that are no longer dependent upon numerical models or empirical relationships.

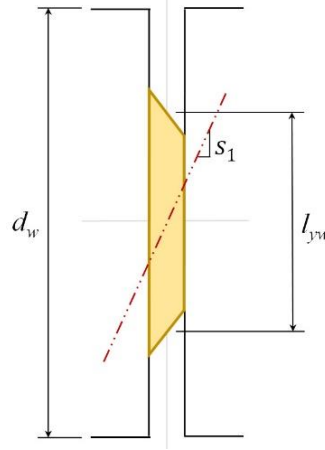


Figure 11: Compression yield stress distribution in the web

5. Comparative Example

The El-Zanaty et al. portal frame (1980) has been used by several researchers as a comparative example because it is one of the most sensitive frames available to test the ability of their method to capture the effects of distributed plasticity on a frame that has little capacity to redistribute forces once yielding has initiated (King et al 1992; Attalla et al 1994; Ziemian et al 2002).

5.1 Nonlinear regression model of the m - p - τ surface

The data that were used to create Fig. 3 were also used to generate nonlinear regression equations for τ in terms of both m and p . As indicated in Figs. 3 and 9, there is a distinct change in the shape of the surface plot when $p > 0.7$. Thus in order to best approximate the full range of values over the m - p - τ surface, the first regression equation was developed for $0 \leq p < 0.7$ and the second for $0.7 \leq p \leq 1.0$. Since the extent of $\tau = 1$ is known with Eq. 1, and the m and p conditions for $\tau = 0$ are known with Eqs. 32 and 33, only the data for $0 < \tau < 1$ were used to determine the regression equations. Based on the results from several trial nonlinear regression models, the one provided in Eq. 35 was found to provide the best r^2 values. With the coefficients as provided in Table 2, $r^2 = 0.99$ ($n = 4,832$) for $0 \leq p < 0.7$ and $r^2 = 0.98$ ($n = 1,042$) for $0.7 \leq p \leq 1.0$.

$$\begin{aligned} \tau = & a_0 + a_1m + a_2m^2 + a_3m^4 + a_4m^6 + a_5m^8 + a_6p + a_7p^2 \\ & + a_8p^4 + a_9p^6 + a_{10}p^8 + a_{11}mp + a_{12}m^2p^2 + a_{13}m^4p^4 \end{aligned} \quad (35)$$

5.2 Stiffness matrix used for modeling the distributed plasticity

Since the bending moments usually vary along the length of the beam-column, the stiffness reduction over the member length must also be accounted for when yielding occurs. An easy and effective way of accomplishing this is to assume the tangent modulus varies linearly over the length of the element. In practice, the error introduced by this assumption is reduced by using multiple elements along the length of the beam-column. The closed-form stiffness matrix

Table 2: Nonlinear regression model coefficients

Coefficients	$0 \leq p < 0.7$	$0.7 \leq p \leq 1.0$
a_0	1.233	-4.976
a_1	-0.9771	-8.224
a_2	1.739	3.425
a_3	-4.870	29.76
a_4	8.364	-76.82
a_5	-5.338	66.64
a_6	1.400	28.48
a_7	-3.863	-38.51
a_8	7.654	29.67
a_9	-12.89	-23.91
a_{10}	7.000	9.239
a_{11}	-2.377	10.26
a_{12}	4.757	-11.78
a_{13}	-13.31	-22.64

developed by Ziemian and McGuire (2002) was chosen for this study because the τ values from Eq. 35 (with coefficients from Table 2) can be used directly for the a and b terms in Eq. 36. The tangent modulus is defined to be $E_{tm} = \tau E$. Since the normalized modulus is E_{tm}/E , then $a = \tau$ using the m and p conditions at the start of the element, and $b = \tau$ using the m and p conditions at the end of the element.

$$[k] = \frac{EI_y}{L} \begin{bmatrix} \frac{12}{L^2} \left(\frac{a+b}{2} \right) & -\frac{6}{L} \left(\frac{2a+b}{3} \right) & -\frac{12}{L^2} \left(\frac{a+b}{2} \right) & -\frac{6}{L} \left(\frac{a+2b}{3} \right) \\ & 4 \left(\frac{3a+b}{4} \right) & \frac{6}{L} \left(\frac{2a+b}{3} \right) & 2 \left(\frac{a+b}{2} \right) \\ & & \frac{12}{L^2} \left(\frac{a+b}{2} \right) & \frac{6}{L} \left(\frac{a+2b}{3} \right) \\ \text{Sym.} & & & 4 \left(\frac{a+3b}{4} \right) \end{bmatrix} \quad (36)$$

5.3 El-Zanaty frame modeled using MASTAN2

The stiffness matrix given in Eq. 36 is already a part of the nonlinear material capabilities of *MASTAN2* (2015). The computer program also contains incremental analysis routines for modeling the nonlinear geometric behavior. Eq. 35 with the coefficients in Table 2 for the W8x31 with minor axis bending was used in the nonlinear material subroutine of *MASTAN2*. Eqs. 32 and 33 were used as the boundaries for $\tau = 0$, and Eq. 1 was used as the limit on the extent of $\tau = 1$.

The El-Zanaty portal frame as depicted in Fig. 12 was modeled using four elements for all three members. The conditions of $p = 0.4$ and 0.6 were investigated by first applying the full vertical load P , then the lateral load was applied in increments up its maximum value of H . The normalized lateral load deflection curves for each condition of p are given in Fig. 12. The maximum lateral load and deflection values for $p = 0.4$ and 0.6 were found to be (0.024,0.34) and (0.007,0.07), respectively. This compares very closely with: approximately (0.018,0.31) and (0.009,0.09) using the plastic zone method by King et al. (1992); approximately (0.020,0.32) and (0.006,0.05) using the proposed model by Attalla et al. (1994); and approximately (0.020,0.39) and (0.008,0.09) using the τ expression proposed by Ziemian et al. (2002).

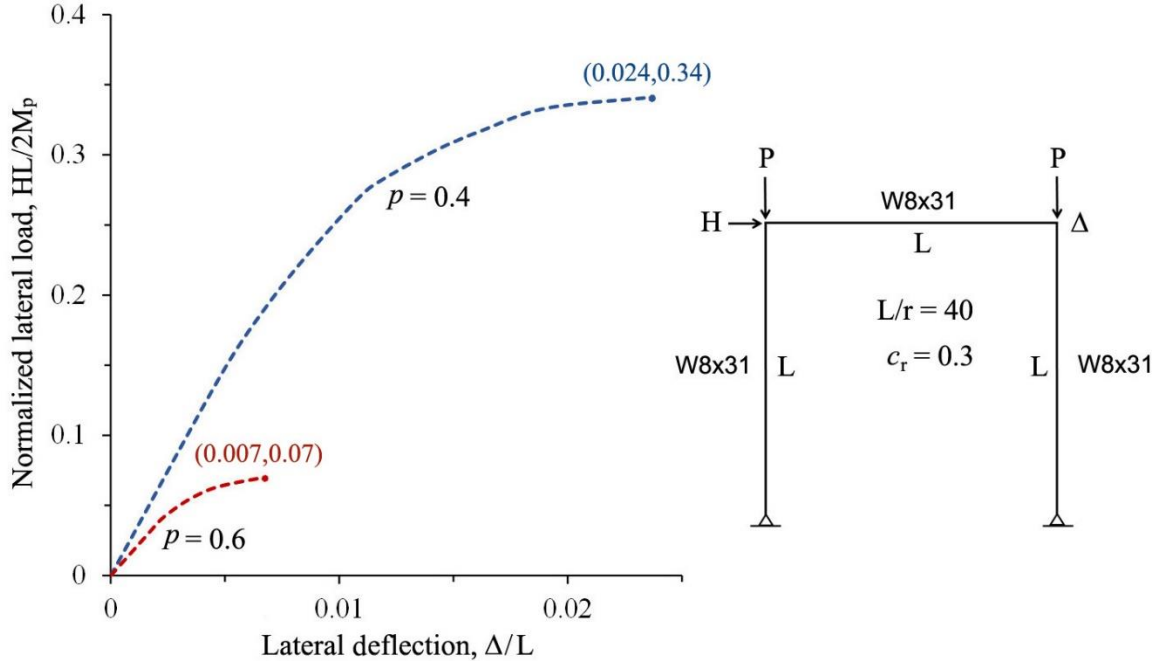


Figure 12: Load deflection curves for El-Zanaty's portal frame with $p = 0.4$ and 0.6

6. Conclusions and Future Research

This research focused on developing a deeper understanding of the stiffness reduction that occurs in W-Shapes with an assumed ECCS residual stress pattern and yielding of the cross-section that occurs due to minor axis bending and axial compression. A detailed model of a W8x31 with 2,046 fiber elements and $c_r = 0.3$ was used to develop a three-dimensional m - p - τ surface plot with 7,590 data points. For the m and p conditions around the perimeter of the surface, analytical expressions for the extent of yielding and stiffness reduction were presented and found to match the fiber element model results to at least three significant digits of accuracy. For the condition of $p = 0$, the analytical expressions with the web excluded were found to be in closed-form and produced results that were in close agreement with those from equations that included the web but required an iterative procedure to obtain the results. For the condition of $m = 0$, the analytical expressions for the extent of yielding and stiffness reduction were found to be in closed-form even with the web included; however the simpler expression for τ with the web excluded also provided a very close approximation. For the conditions of $p = 0.2, 0.5$ and 0.75 , the stress distributions in the flanges and web illustrated the progression of seven elasto-plastic stress states as m was increased from the initial yield condition to the fully plastic condition. The results indicated that for a given increment of m from the initial yield condition, the loss of stiffness occurs more rapidly as p is increased, and the loss of stiffness occurs most rapidly for all conditions of p when the flanges yield in both compression and tension. The data used to produce the m - p - τ surface plot were also used to develop two nonlinear regression models for τ of a W8x31 with $c_r = 0.3$. The regression equations for τ were used as normalized tangent modulus expressions in *MASTAN2* and were found to provide load deflection results that were in close agreement with published results for the El-Zanaty portal frame.

Future research will include studying the effects of simplifying the m - p - τ surface plot for more practical use. Since the closed-form stiffness matrix in *MASTAN2* assumes a linear variation in the

tangent modulus along the length of the element, developing an appropriate linearization of the 3D surface would be a consistent approach. The m - p - τ surface plot clearly indicates two distinct regions of stiffness reduction: the first is between stress state 0 (at the extent of $\tau = 1$) and stress state 8; and the second is between stress state 7 and stress state 8. Based on the conclusions made concerning the rapid loss in stiffness at the onset of stress states 2, 4 and 6, the m - p - τ conditions at these points on the surface would potentially provide the best intermediate values for joining two linear expressions. If successful at producing reasonably accurate results with this approach, the methodology would then be extended to investigate bi-axial bending conditions.

References

- Attalla M.R., Deierlein G.G., McGuire W. (1994). "Spread of plasticity: quasi-plastic-hinge approach." *Journal of Structural Engineering*, 120 (8) 2451-2473.
- Chen W.F., Sohal I. (1995). *Plastic design and second-order analysis of steel frames*. Springer-Verlag, New York.
- ECCS (1984). "Ultimate limit state calculation of sway frames with rigid joints." *TC 8 of European Convention for Constructional Steelwork (ECCS)*, No. 33.
- El-Zanaty M.H., Murray D.W., Bjorhovde R. (1980). "Inelastic behavior of multistory steel frames." *Structural Engineering Report No. 83*, University of Alberta, Edmonton, Alberta, Canada.
- King W.S., White D.W., Chen W.F. (1992). "Second-order inelastic analysis methods for steel-frame design." *Journal of Structural Engineering*, 118 (2) 408-428.
- Kucukler M., Gardner L., Macaroni L. (2014). "Stiffness reduction method for the design of steel columns and beam-columns." *Proceedings of the 2014 SSRC Annual Stability Conference*, Toronto, Canada.
- Kucukler M., Gardner L., Macaroni L. (2014). "A stiffness reduction method for the in-plane design of structural steel elements." *Engineering Structures*, 73 (5) 72-84.
- White D.W., Liew Y.J.R., Chen W.F. (1991). "Second-order inelastic analysis for frame design: A report to SSRC Task Group 29 on recent research and the perceived state-of-the-art." *Structural Engineering Report CE-STR-91-12*, Purdue University, West Lafayette, Indiana.
- Ziemian R.D., McGuire W. (2002). "Modified tangent modulus approach, a contribution to plastic hinge analysis." *Journal of Structural Engineering*, 128 (10) 1301-1307.
- Ziemian R.D., McGuire W. (2015). *MASTAN2*, Version 3.5.
- Ziemian R.D., Miller A.R. (1997). "Inelastic analysis and design: frames with members in minor-axis bending." *Journal of Structural Engineering*, 123 (2) 151-156.
- Zubydan A.H. (2011). "Inelastic second order analysis of steel frame elements flexed about minor axis." *Engineering Structures*, 33 (4) 1240-1250.